Materials Research Express

PAPER

Comparing half-metallic, MOKE, and thermoelectric behavior of the CrTiZ (Z = As, P) half-Heuslers: a DFT study

M Sadeghi[1], A Zelati[2], A Boochani[3], A Arman[4] and S Mirzaei[5]

[1] Mälardalens Högskola(EST), Mälardalen University, Vasteras, Sweden
[2] Department of Basic Sciences, Birjand University of Technology, Birjand, Iran
[3] Department of Physics, Kermanshah Branch, Islamic Azad University, Kermanshah, Iran
[4] ACECR, Vacuum Technology Research Group, Sharif University Branch, Tehran, Iran
[5] CEITEC BUT, Brno University of Technology, Purkynova 123, CZ-61200, Brno, Czech Republic

E-mail: saeed.mirzaei@ceitec.vutbr.cz

OPEN ACCESS

RECEIVED
12 March 2021

REVISED
8 April 2021

ACCEPTED FOR PUBLICATION
12 April 2021

PUBLISHED
21 April 2021

Keywords: CrTiZ (Z = As, P), Half-Heusler compounds, DFT, electronic properties, thermoelectric properties

Abstract

Structural, half-metallic, magneto-optic, and thermoelectric properties of CrTiZ (Z = As, P) half-Heusleres compounds are investigated based on density functional theory. These compounds have mechanical stability in the ferromagnetic state with a high bulk modulus. They are often half-metallic with a large and integer magnetic moment and are very attractive in spintronics, magneto-optics applications. The magnetic moments of CrTiAs and CrTiP were 2.9865 μ_B and 3.00 μ_B, respectively, which were attributed to their ferromagnetic phase. Additionally, the positive sign of the phonon branches indicates the dynamic stability of these compounds. Applying both GGA and mBJ approximations, CrTiAs and CrTiP compounds exhibited a half-metallic nature by 100% spin polarization. The Kerr angle obtained from magneto-optic results demonstrated a high-intense peak for these compounds in the visible edge with a negative sign. Eventually, a figure of merit with a value above the room temperature was found for both compounds in which the holes are charge carriers.

1. Introduction

For the first time in 1983, Groot *et al* predicted the half-metallic behavior of two ternary ferromagnetic compounds, namely NiMnSb and PtMnSb [1, 2]. The Density Functional Theory (DFT) calculations were performed to investigate their band structures that have hybrid characteristics. These compounds behave differently in two spin states, where, in the minority spin state, they exhibit semiconducting behavior while metallic behavior is dominant in the majority spin state. The 100% spin polarization is due to the hybrid characteristics of NiMnSb and PtMnSb compounds at the Fermi surface. The complete spin polarization current was expanded by such compounds as Heuslers, which are suitable cases for spintronic devices and magneto-optic applications.

The half-metal ferromagnetic property has been attracting considerable interest, which led to the development of new materials with potential applications in optoelectronic, magneto-electronic, spintronic devices, and nanomaterials [1, 2]. Meanwhile, magnetic materials have emerged as an essential group of materials due to their application in spintronics, magneto-optics, and magnetic memories. In this regard, thanks to their ferromagnetic and half-metallic properties, Heusler compounds are suitable candidates for the abovementioned industries. Three different kinds of Heusler compounds include full, half, and inverse Heusler alloys. The formula for half-Heusler, full-Heusler, and inverse Heusler are XYZ, X_2YZ, and XYXZ, respectively, in which X and Y are high and low valance transition metals and Z is sp electron element.

In recent years, there has been a surge of interest in structural and electronic properties of half-Heusler combinations such as PtBiZ (Z = Fe, Mn, Ni, Co) and PdMnBi [3, 4]. The half-metallic of several different half-Heusler compounds have been studied in [5, 6]. In addition, optoelectronic properties of RbSrZ(Z = C, Si, Ge), CoCrZ(Z = Al, Ga), NiTiX and CoVX(X = Sb, Sn) have been investigated in [7–9], respectively. The

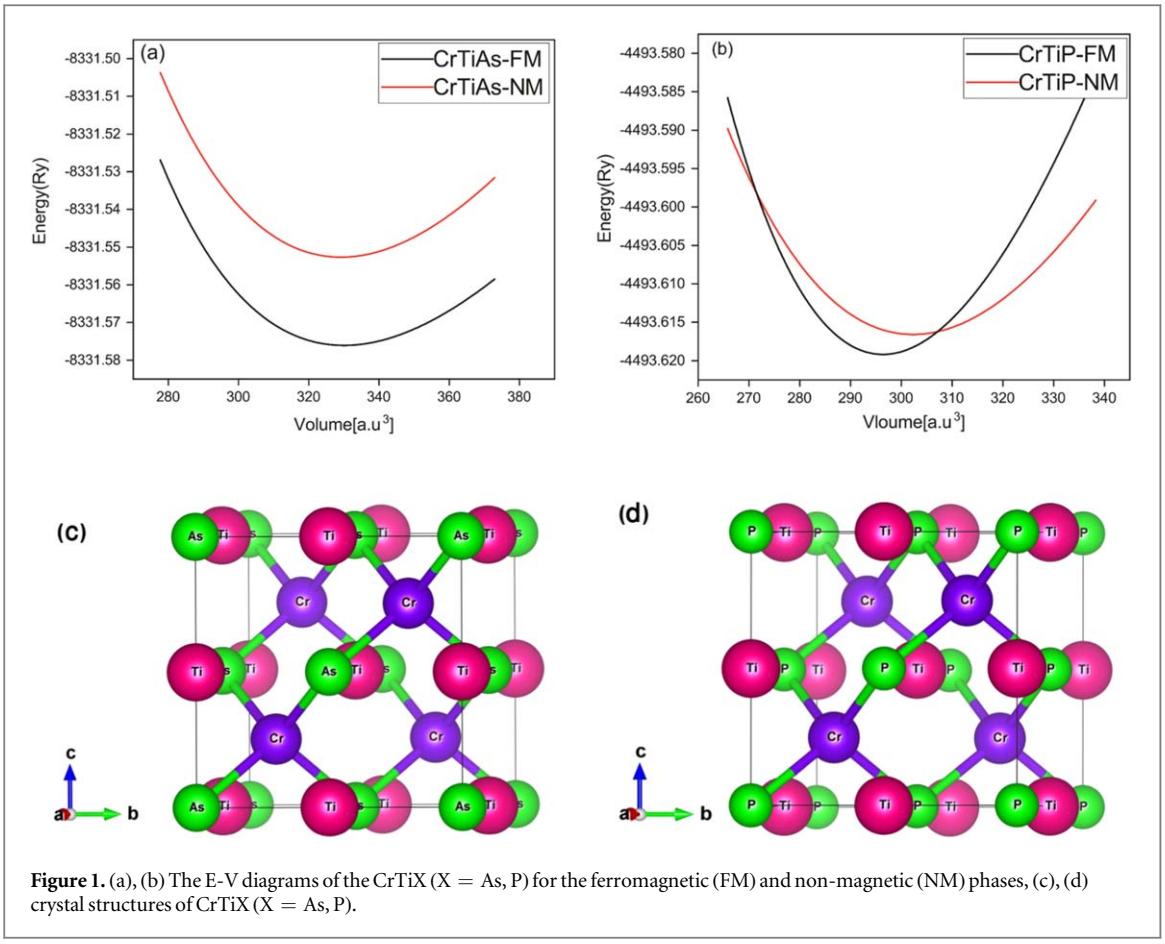

Figure 1. (a), (b) The E-V diagrams of the CrTiX (X = As, P) for the ferromagnetic (FM) and non-magnetic (NM) phases, (c), (d) crystal structures of CrTiX (X = As, P).

mechanical and half-metallic behavior of RhCrZ(Z = Si, Ge) half-Heusler compounds have been examined in [10]. Recently, the half-metallic and optical properties of the two CrTiZ (Z = As, P) compounds have been investigated. Calculations showed that these two compounds have elastic stability and have 100% spin polarization at the Fermi level [11].

Materials with small band gaps are required for cooling applications, while for power generations, materials with large gaps are more appropriate. Because at higher temperatures, larger gaps (larger E_g) will result in greater ZT. For thermoelectric applications, half-Heusler alloys with a high power factor, good mechanical properties, low-cost synthesis, and good thermal stability [12–15] have been investigated recently. However, due to the high lattice thermal conductivity (10 W/mK) and low ZT, compared to other investigated materials, such as ternary or quaternary chalcogenide compounds including Cu_3SbX_4 (X = Se, S) and $CuGaTe_2$ [16, 17], have been obsolesced. Among the useful and applicable thermoelectric materials, the n-type compounds of MNiSn (M = Zr, Hf) or p-type alloys of XCoSb (X = Ti, Zr, Hf), in which the value of their ZT is about 1, can be mentioned.

Furthermore, some ferromagnetic semi-metals such as $Co_2TiAl_{0.75}Si_{0.25}$ have shown a high Seebeck coefficient of about 63 μV/K at 750K [18–23]. These materials generally have ceramic behavior and brittle nature, thus prone to crack, which often degrades their performance and lifetime [24]. Whereas the Heusler compounds we study in this work are ductile and therefore ideal for thermoelectric applications. Co, Rh, V, and Si atoms from IX-V-IV groups of the periodic table, can form distinct compounds with appealing physical properties.

We employed the DFT calculations to expand the current knowledge on the magneto-optical and thermoelectric, and electronic properties of CrTiAs and CrTiP compounds. In this regard, calculations were followed by Wien2K, Quantum Espresso, and BoltzTraP packages. First, mechanical stability from the statical and dynamical views was performed, then the half-metallic properties were investigated. Ultimately, the magneto-optical and thermoelectric behaviors were studied.

2. Computational details

The structural, half-metallic, and thermoelectric properties of CrTiZ (Z = As, P) compounds were studied based on density functional theory (DFT) [25–28]. The Kohn–Sham equation was approximated by full

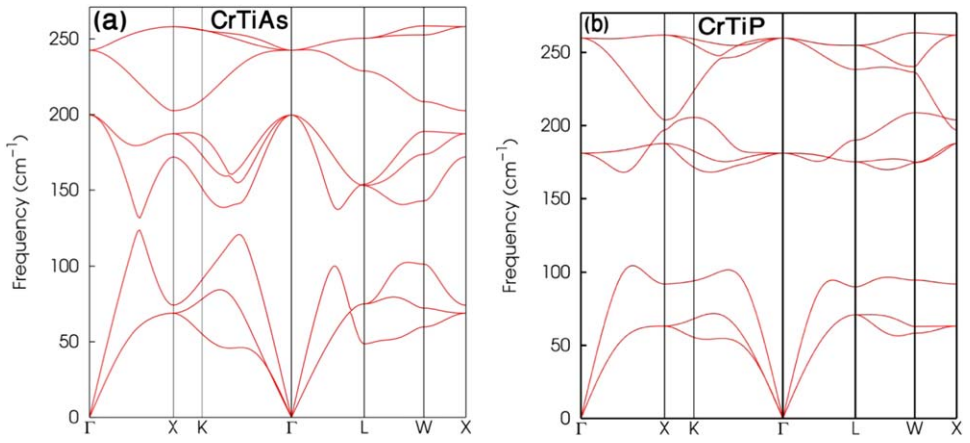

Figure 2. phonon scattering in the first Brillouin zone for CrTiX (X = As, P) compounds.

Table 1. The lattice constant a (A°), magnetic moment μ_B (Bohr magneton), bulk modulus B (GPa), the derivative of Bulk modulus B', equilibrium volume V (Bohr-3) and total energy in equilibrium volume E (Ryd) of CrTiAs and CrTiP compounds.

Compound	a (A°)	μ_B	B′	B (GPa)	V (Bohr^3)	E (Reyd)
CrTiAs	5.8044	2.9865	5.5834	120.2255	329.9128	8331.5760
CrTiP	5.6377	3.00	3.9588	144.5925	302.3041	443.61659

potential augmented plane waves plus local orbitals (FP-LAPW+lo), and the exchange-correlation potential was solved with GGA and mBJ approximations [29, 30]. The electronic and thermoelectric properties results were extracted from the Wien2K code and the phonon one from Quantum Espresso [31–33]. The input parameters as K-point, RKmax, and lmax in the Wien2K calculations were selected to 4000, 8.5, and 10, respectively. The Ecut and K-point in the Quantum Espresso were optimized to 150 and 14 × 14 × 14, respectively. Also, for calculating the Magneto-Optik-Kerr-Effect (MOKE), we used the exciting code [34], and for increased accuracy, the input KPoint was selected to 20 × 20 × 20.

3. Results and discussion

3.1. Structural properties

Crystal structures of unit cell volume diagrams in terms of their total energy variations contain essential information about the structural properties and the static equilibrium crystals. Figure 1 depicts the optimized energy as a function of volume (E-V) for CrTiAs and CrTiP compounds in ferromagnetic and non-magnetic phases, calculated based on Brinch-Marnagon's equation. Although both phases were mechanically stable, it was found that these compounds are more stable in the ferromagnetic phase than the non-magnetic phase, which can be attributed to the fact that the equilibrium volume energy of these compounds in the ferromagnetic phase is lower. As can be seen in figure 1(a), the E-V curves of CrTiAs do not intersect; therefore, a phase transition under pressure was not expected for this alloy. Contrarily, a phase transition in the volume of 350 Bohr^{-3} was observed for the CrTiP compound (figure 1(b)), above which the non-magnetic phase is more stable compared to the magnetic phase. These results indicate that the CrTiP compound transits to the non-magnetic phase under strain. It should be mentioned that the magnitude of the magnetic to non-magnetic phase transition pressure was calculated to be 56.3 GPa. The detailed information of the E-V diagram for these two CrTiAs and CrTiP compounds is listed in table 1. The results show that the lattice constants of these compounds correspond to other work performed by GGA approximation.

The crystal structure of CrTiAs and CrTiP in $F\bar{4}3m$ space group are depicted in figures 1(b) and (c). The As and P are located in (0, 0, 0), Cr in (1/4, 1/4, 1/4), and Ti in (1/2, 1/2, 1/2) positions.

The phonon scattering in the first Brillouin zone can represent the dynamical stability of the systems and other important information on the mechanical and thermal behavior of crystal structures. Figure 2 shows that the phonon scattering in CrTiAs and CrTiP compounds has a positive sign, indicating the dynamic stability of these structures. It was observed that in both compounds, particularly in the CrTiAs, the slope of phonon levels at the Γ point represented a Dirac shape, noting that the capacity of these two compounds is very high, and the

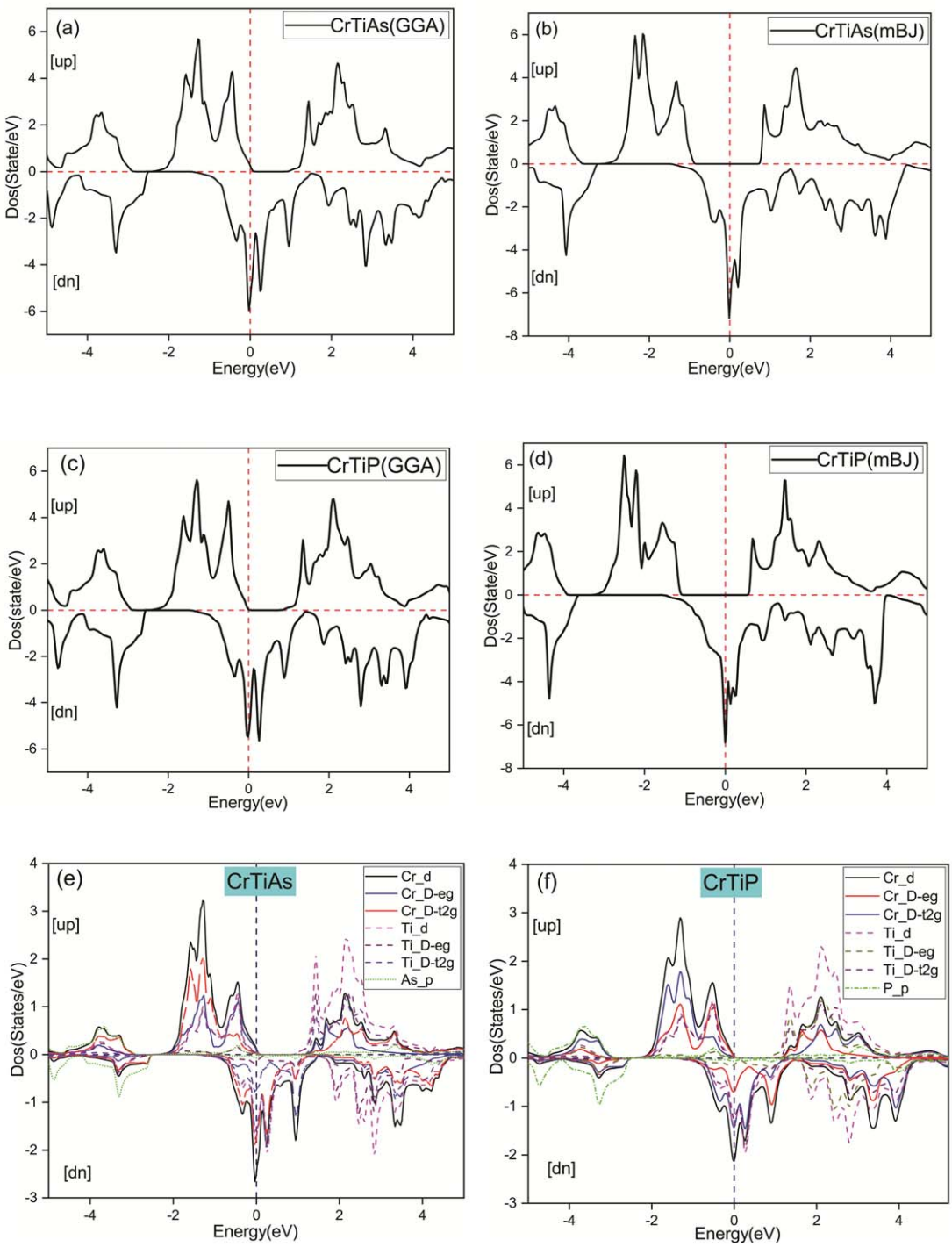

Figure 3. (a)–(d) The DOS of the CrTiZ (Z = As, P) compounds by GGA and mBJ approximations, and (e), (f) are the partial DOS for two up and down spins.

heat transfer is well performed at low temperatures. It can be seen that there is a significant vibrational gap from the frequency of 100 cm^{-1} to 160 cm^{-1} in the CrTiP compound; therefore, no vibrational energy was observed in this region. On the other hand, at higher frequencies in the infrared (IR) region, a fast energy transfer in the directions of X, K, Γ was observed. For the CrTiAs compound in the 125 cm^{-1} and 200 cm^{-1} frequencies, there are two small band gaps in which the former is direct, and the other is indirect. Therefore, energy transfer and absorption in these areas occur with a short delay in the IR region, wherein the light absorption in the 200 cm^{-1} frequency region faces a gap. Eventually, it can be concluded that despite the static and dynamic stability and the similarity of their atoms, CrTiP and CrTiAs compounds exhibited different thermal and optical behavior due to the presence of two different P and As atoms in their structure. The presence of longitudinal gradients of phonon

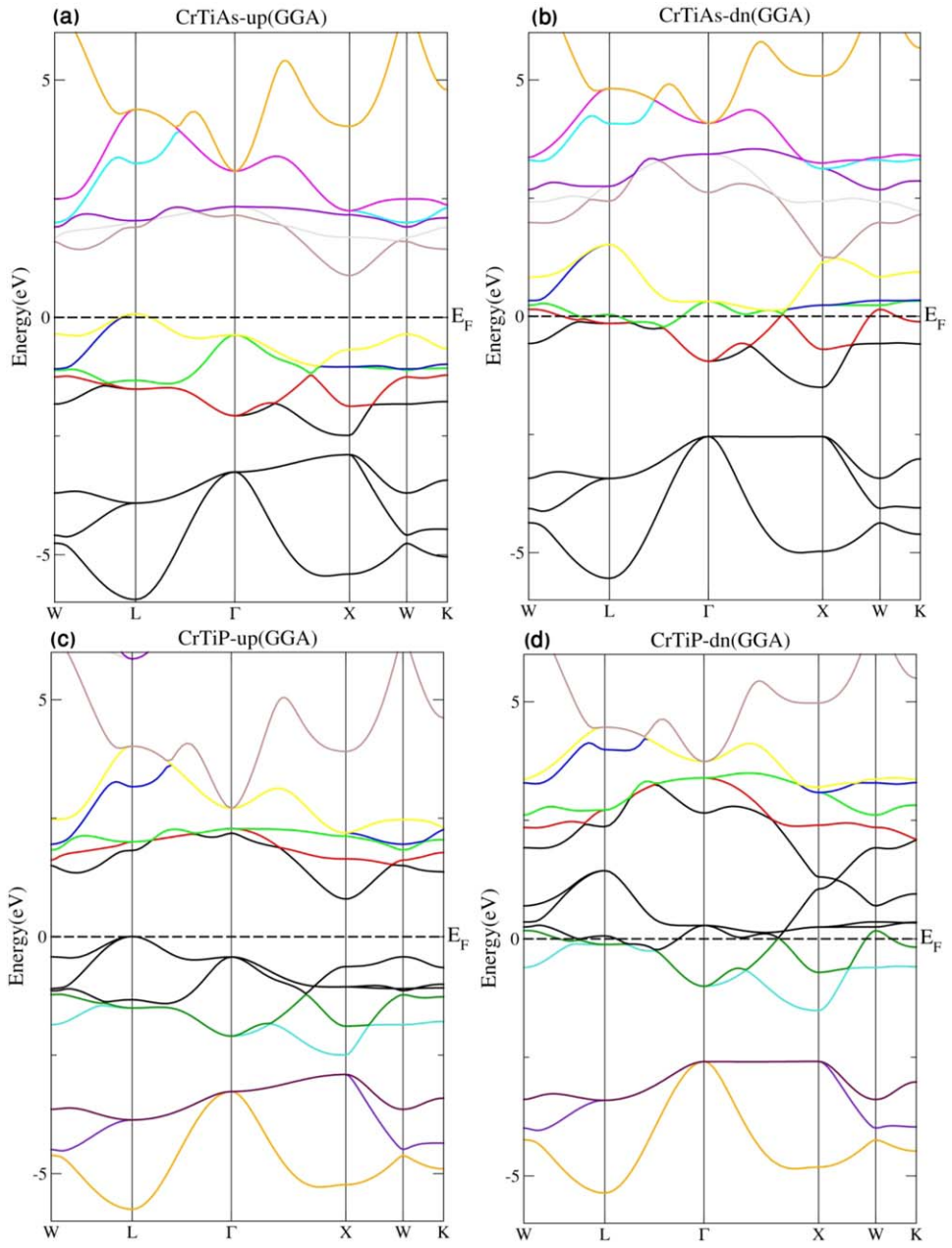

Figure 4. The band structure of CrTiZ (Z = As, P) compounds in GGA and mBJ approximations for two up and down spins.

energy levels in the range of 0 cm^{-1} to 200 cm^{-1} in the CrTiAs compound indicates that this compound is an exemplary transducer for the thermal and optical energies.

3.2. Electronic properties

Figure 3 shows the density of electronic states (DOS) for compounds CrTiZ (Z = As, P) in both up and down spin states with two GGA and mBJ approximation. It was found that in the CrTiAs compound with GGA approximation, there was a 95% spin polarization, while with mBJ approximation, it reached 100%. Note that the anisotropy can be seen at Fermi level for both approximations, wherein minority spin state it exhibited entirely metallic while in majority spin state showed semiconductor characteristics. By applying mBJ approximation, the valance electron states were shifted to lower energies, which led to an increased bandgap from 1.5 eV to 2.5 eV in mBJ. It is noteworthy that in both compounds with the GGA approximation, all spin gaps are flip.

Partial DOS diagrams of CrTiZ (Z = As, P) compounds in figures 3(e) and (f) show that the critical factor of the electronic states splitting in the majority spin state was the interaction of Ti D-2g and Ti D-e.g. with Cr D-e.g. and Cr D-2g orbitals. It also demonstrates that in the semiconductor state, the electronic states below the Fermi surface often belong to Cr-d and somehow to Ti-d degeneracy. Nonetheless, above the Fermi surface, the

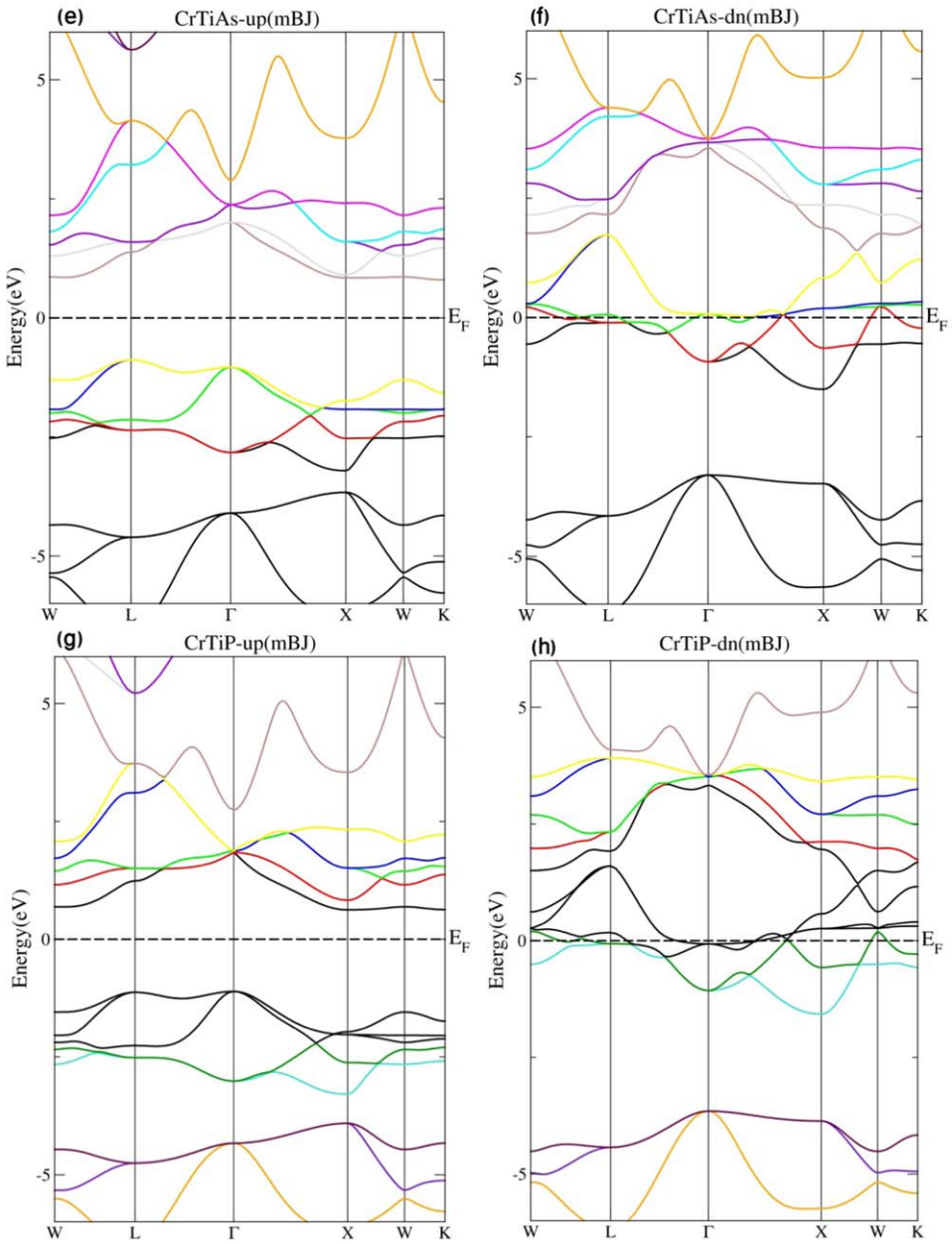

Figure 4. (Continued.)

electronic states belong to the Ti-d degeneracy; thus, these orbitals play a vital role in electronic conduction. Furthermore, in the minority spin state, Cr-d and Ti-d orbitals are the main factors in conductivity. Electronic states of As-p and P-p orbitals in CrTiAs and CrTiP compounds, respectively, were between −5 eV to −3 eV regions and generally did not contribute to conduction. The overlap of the electronic states in the Fermi region was associated with d-d electronic bonds in these compounds.

Figure 4 shows the calculated electronic band structure of CrTiAs and CrTiP compounds in two spin states. It was revealed that the compound CrTiAs in the up-spin state was a p-type semiconductor with a direct bandgap of 0.88 eV, in which the maximum valance and minimum conduction were at L and X points, respectively. Although in the valance and conduction regions near the Fermi surface, the gradient of energy levels was negligible, in the regions of $+5 <$ eV and < -5 eV, in the symmetric directions of Γ and W, the energy gradients were significantly increased. Consequently, electron mobility was considerable for electrons with energies above 2.5 eV. On the other hand, in the down-spin state of the CrTiAs compound, it was observed that the valance electron states shifted towards the Fermi surface, where at point X, two states intersect and are in displacement (see figures 4(b), (f)). This observation can be attributed to the topological behavior of the CrTiAs compound. As discussed earlier, the electron states that intersect the Fermi surface were all S-like and P-like atoms of Ti-d and Cr-d orbitals. Similar behavior was observed for the CrTiP compound, where the valance

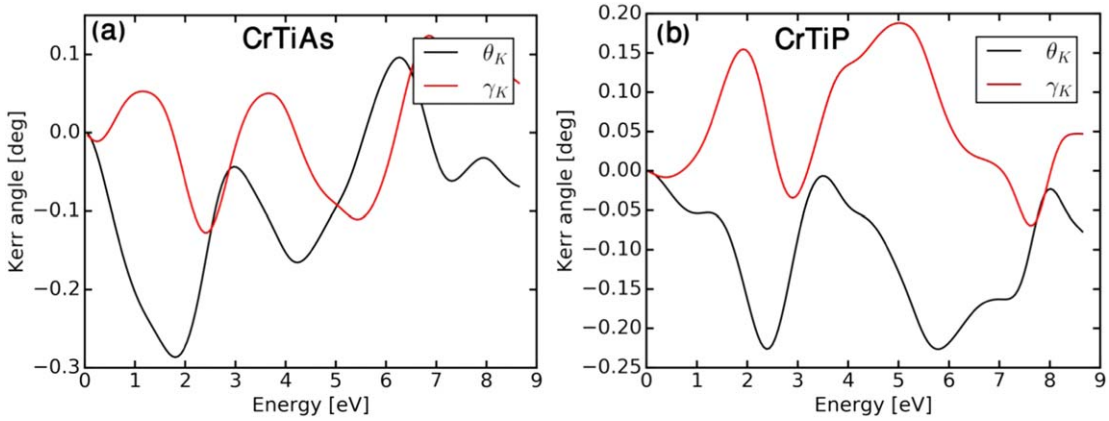

Figure 5. The Kerr angle (θ_K) and ellipticity (γ_K) of (a) CrTiAs and (b) CrTiP compounds versus optical energy.

region was shifted in the down-spin state and moved towards the Fermi surface, then the electron states were displaced along X-W symmetric path. Therefore, it can be concluded that CrTiAs and CrTiP compounds are proper candidates for topological behavior in addition to spintronic behavior. In the following, we calculated the band structure of these compounds with mBJ approximation. The effects of this approximation have shifted the valance region to lower energies in CrTiAs. Here again, we see an indirect bandgap with a magnitude of 1.76 eV, wherein down-spin state not only the gradients of the electronic states are increased along the Γ -X and Γ -L paths, but also the electronic states, especially in the symmetric path of X-W are in displacement. Similarly, in the down-spin state of CrTiP, the mobility of electrons is significantly increased, and the topological behavior is observable. The mBJ approximation transformed the CrTiP compound in the up-spin state to an n-type semiconductor, in which the majority of carrier charges are electrons.

3.3. MOKE effect

When a linearly polarized light (phonons) reflects from the surface of a magnetic material, the polarization plane of light is rotated due to spin–orbit interaction, known as the magneto-optical Kerr effect (MOKE). The so-called Kerr angle is the rotation angle of the direction of reflected phonons with respect to the original polarization. The relative geometry of the flat surface, the orientation of magnetization, and the direction of wave vector of incoming phonons define the value of Kerr angle. Although extensive research has been carried out to study the Kerr effect, there is scant information on the Kerr effect of CrTiAs and CrTiP compounds. The polar Kerr effect is investigated in which both the incoming wave vector and magnetization are perpendicular to the surface. In this effect, the polar Kerr angle is a complex angle, thus is formulated according to macroscopic conductivity tensor. Here, we considered cubic systems in which the direction of magnetization is parallel to the *z*-axis; hence the Kerr angle is given by:

$$\Phi_K = \theta_K + i\gamma_K = \frac{-\delta_{xy}}{\delta_{xx}\sqrt{1 + i\left(\frac{4\pi}{\omega}\right)\delta_{xx}}} \tag{1}$$

where θ is the real Kerr-rotation angle, γ_K is the Kerr ellipticity, and σ_{xx} and σ_{yy} are components of the optical conductivity tensor. The components of macroscopic conductivity tensor can be associated with microscopic optical transitions by the Kubo formula. The calculations were performed according to the data provided by Langlinais and Callway [35]. Whenever the plane-polarized phonons are reflected from or transmitted through a matter with nonzero magnetization, they can be elliptically polarized. These reflection and transference effects are called the magneto-optical Kerr effect and magneto-optical Faraday effect, respectively [36, 37]. Both of these effects are zero not only if there is no spin polarization but also in the absence of spin–orbit interaction. As a result of the withdrawal of time-reversal symmetry for the complete system, it will be a sensitive examination of relativistic energy band theory.

Figure 5(a) shows the real part, and figure 5(b) shows the imaginary part of the Kerr effect (Kerr ellipticity) for CrTiAs and CrTiP compounds. The optical conductivity tensor can be written as:

$$\sigma = \begin{pmatrix} \sigma_{xx} & \sigma_{xy} & 0 \\ -\sigma_{xy} & \sigma_{xx} & 0 \\ 0 & 0 & \sigma_{zz} \end{pmatrix} \tag{2}$$

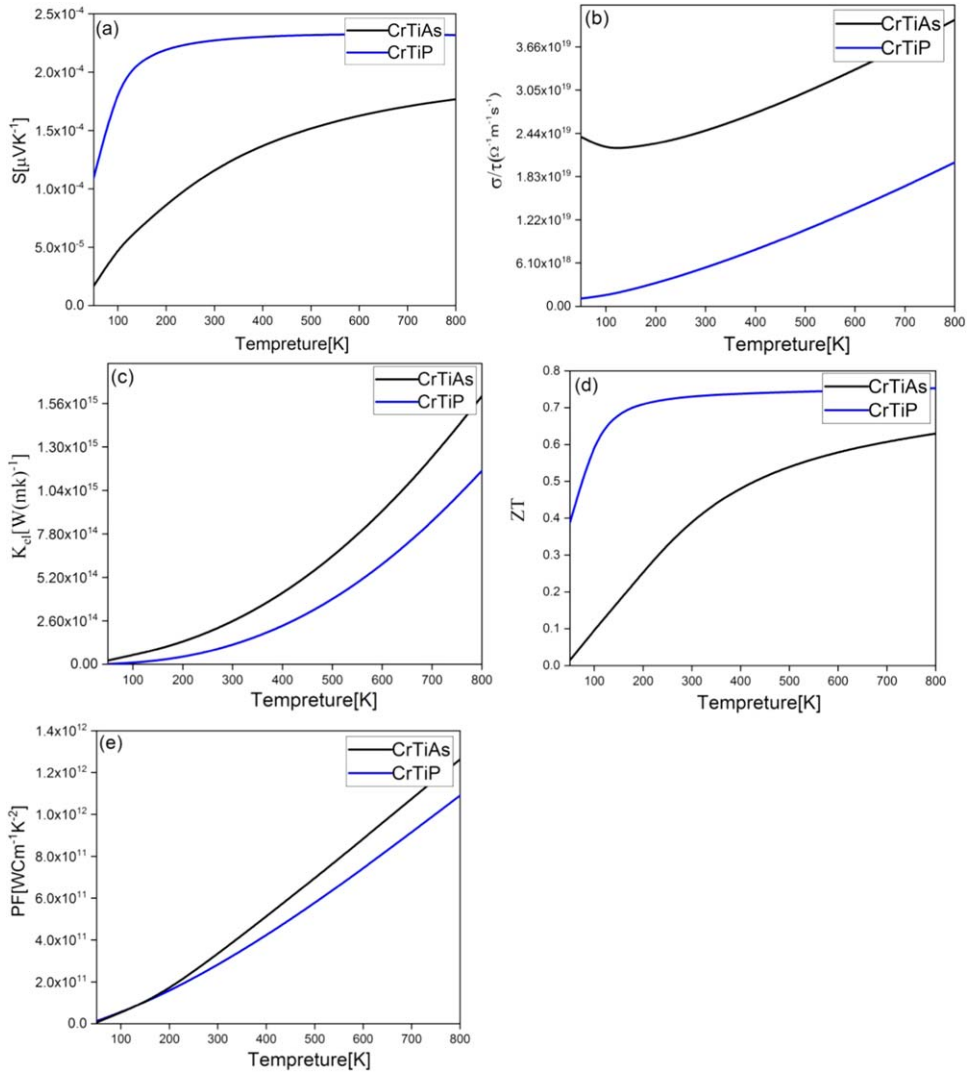

Figure 6. Temperature dependence of the (a) Seebeck coefficient, (b) electrical conductivity, (c) Thermal conductivity (d) figure of merit(ZT), and (e) power factor (PF) in the range of 50–800 K for CrTiZ (Z = As, P) compounds.

Since these compounds exhibit 100% spin polarization and their half-metallic behavior, their magnetic moment (see table 1), according to the magneton Bohr, follows Pauli-Slater's law. Therefore, we expect that whenever the electromagnetic spectrum of light falls on the surface of CrTiAs and CrTiP, the magnetic component of light interacts with the magnetic moment of these compounds. Therefore, the polarization of light is visible due to the reflection of phonons from their surface. Furthermore, considerable changes of Kerr angles θ and η were found in these two compounds. It was observed that the CrTiAs has a very good θ at the edge of visible light, with a negative peak sign, which indicates the counterclockwise polarization direction of the light, and also in this area of θ, a polarization has occurred in the light. Two other peaks, one in the negative region and the other in the positive region, appeared in the energies of 4.2 eV and 6.3 eV, respectively, which shows that by increasing the energy of the reflected photon, the rotation of the electronic field of reflected light changed from the counterclockwise to the clockwise as well as its polarization. Therefore, from the visible edge to the energy of 6.3 eV, a change in the nature of its polarization and magnitude was observed.

In contrast to CrTiAs, the nature of polarization in the CrTiP compound was consistent, and we see two peaks, one in 2.4 eV and the other in 5.8 eV, whose sign is negative. Therefore, the electric field rotation in both states is counterclockwise, and polarization in this region is high due to the peaks of η in both combinations. As a result, with the increase in the energy of the incoming photon in these compounds, the type and amount of polarization changes, which shows that these two compounds are used in the magneto-optic industry.

3.4. Thermoelectric properties

There has been substantial research undertaken on thermoelectric materials due to their capability of converting thermal energy to electric energy and reciprocally, based on Seebeck and Peltier effects [38–41]. The

thermoelectric efficiency of materials can be measured by calculating the dimensionless figure of merit ZT, given by:

$$ZT = \frac{S^2 \delta T}{K} \tag{3}$$

where T is the absolute temperature, S is the Seebeck coefficient (thermopower), σ is the electrical conductivity, and K is the thermal conductivity, which includes the lattice and electron portion [42, 43]. According to this relation, the excellent thermoelectric materials must exhibit a high Seebeck coefficient and electronic conductivity and a low lattice thermal conductivity. However, increasing the value of σ and density of charge carriers often leads to an increase in the thermal conductivity of the electrons, which consequently deteriorates the performance of the thermoelectric materials. Therefore, the selection and design of proper thermoelectric materials depend on essential parameters such as the size of the bandgap, shape and width of the gap near the Fermi surface, effective mass, and mobility of carriers.

Figure 6(a) depicts the plot of the Seebeck coefficient for CrTiZ (Z = As, P) compounds, which is positive in both cases, indicating that the holes are the transport factor. However, the Seebeck coefficient was smoothly enhanced by increasing the temperature of the CrTiAs compound, while in the case of CrTiP, after an abrupt increase, it was constant above the temperature of ~200 K. A similar behavior was observed for the electrical conductivity of these two compounds (figure 6(b)) where the conductivity was almost linearly increased above 100 K. Correspondingly, the thermal conductivity of the compounds were also exhibited a similar trend, as shown in figure 6(c), in which the profile of thermal conductivity was parabolic up to 500 K, while a linear dependence was fount above 500 K. This results pointed out that at higher temperatures more electron and hole pair contributed to conduction. Additionally, no conductivity was detected for CrTiAs below 50 K, while in the case of CrTiP, a conduction gap was found at low temperatures. This slight discrepancy was attributed to the difference in the semi-conductivity of the two compounds. Figure 6(d) shows the figure of merit for CrTiAs and CrTiP compounds in which the profiles are similar to Seebeck coefficient plots where saturation occurred for CrTiP above ~200 K. Note that the rate of increase in the figure of merit for CrTiAs was also declined at high temperatures. It can be concluded that the CrTiP compound exhibited thermoelectric characteristics at low temperatures higher figure of merit at room temperature compared to CrTiAs. Therefore, these findings suggest that CrTiP is a proper candidate for thermoelectric applications at room temperature as well as at elevated temperatures. Additionally, since the power factor (PF) of these two compounds was steadily increased with temperature, it can be therefore stated that CrTiAs and CrTiP compounds are suitable for power generator purposes.

4. Conclusion

The structural, half-metallic, magneto-optical, and thermoelectric properties of CrTiX (X = As, P) compounds were investigated based on DFT. Structural calculations showed that these compounds are more stable in the ferromagnetic phase. Phonon calculations also revealed that these compounds are stable under lattice vibrations. These compounds with GGA and mBJ approximations in all conditions are ferromagnetic half-metals with a large magnetic moment, 2.9865 μ_B and 3.00 μ_B for CrTiAs and CrTiP, respectively. The highest magneto-optical response of the CrTiAs compound occurred at energies of 1.9 eV and 6.1 eV, with the difference that in the former, the electric field rotation occurred to the right, and in the latter, the polarization occurred to the left. The CrTiPcompound possessed a larger Seebeck and figure of merit coefficient and exhibited good thermodynamic stability at elevated temperatures.

Acknowledgments

We acknowledge CzechNanoLab Research Infrastructure supported by MEYS CR (LM2018110).

Data availability statement

The data that support the findings of this study are available upon reasonable request from the authors.

ORCID iDs

M Sadeghi https://orcid.org/0000-0002-6978-2771
A Boochani https://orcid.org/0000-0002-2383-4169

S Mirzaei https://orcid.org/0000-0002-1905-4741

References

[1] de Groot R A, Mueller F M, Engen P G V and Buschow K H J 1983 New class of materials: half-metallic ferromagnets *Phys. Rev. Lett.* **50** 2024–7

[2] De Boeck J, Van Roy W, Motsnyi V, Liu Z, Dessein K and Borghs G 2002 Hybrid epitaxial structures for spintronics *Thin Solid Films* **412** 3–13

[3] Huang W, Wang X, Chen X, Lu W, Damewood L and Fong C 2014 Structural and electronic properties of half-Heusler alloy PdMnBi calculated from first principles *Mater. Chem. Phys.* **148** 32–8

[4] Huang W, Wang X, Chen X, Lu W, Damewood L and Fong C 2015 Structural and electronic properties of half-Heusler alloys PtXBi (with X = Mn, Fe, Co and Ni) calculated from first principles *J. Magn. Magn. Mater.* **377** 252–8

[5] Guan-Nan L and Ying-Jiu J 2009 First-principles study on the half-metallicity of half-heusler alloys: XYZ (X = Mn, Ni; Y = Cr, Mn; Z = As, Sb), Chinese *Phys. Lett.* **26** 107101

[6] Rozale H, Amar A, Lakdja A, Moukadem A and Chahed A 2013 Half-metallicity in the half-Heusler RbSrC, RbSrSi and RbSrGe compounds *J. Magn. Magn. Mater.* **336** 83–7

[7] Ahmad M, Murtaza G, Khenata R, Omran S B and Bouhemadou A 2015 Structural, elastic, electronic, magnetic and optical properties of RbSrX (C, SI, Ge) half-heusler compounds *J. Magn. Magn. Mater.* **377** 204–10

[8] Missoum A, Seddik T, Murtaza G, Khenata R, Bouhemadou A, Al-Douri Y, Abdiche A, Meradji H and Baltache H 2014 *Ab initio* study of the structural and optoelectronic properties of the half-Heusler CoCrZ (Z = Al, Ga) *Can. J. Phys.* **92** 1105–12

[9] Ameri M, Touia A, Khenata R, Al-Douri Y and Baltache H 2013 Structural and optoelectronic properties of NiTiX and CoVX (X = Sb and Sn) half-Heusler compounds: an *ab initio* study *Optik* **124** 570–4

[10] Mehmood N, Ahmad R and Murtaza G 2017 *Ab Initio* investigations of structural, elastic, mechanical, electronic, magnetic, and optical properties of half-heusler compounds RhCrZ (Z = Si, Ge) *J. Supercond. Novel Magn.* **30** 2481–8

[11] Ahmad R, Mehmood N and First A 2018 Principle study of half-heusler compounds CrTiZ (Z = P, As) *J. Supercond. Novel Magn.* **31** 257–64

[12] Chen S and Ren Z 2013 Recent progress of half-Heusler for moderate temperature thermoelectric applications *Mater. Today* **16** 387–95

[13] He R, Gahlawat S, Guo C, Chen S, Dahal T, Zhang H, Liu W, Zhang Q, Chere E and White K 2015 Studies on mechanical properties of thermoelectric materials by nanoindentation *Physica Status Solidi (a)* **212** 2191–5

[14] Huang L, Zhang Q, Yuan B, Lai X, Yan X and Ren Z 2016 Recent progress in half-Heusler thermoelectric materials *Mater. Res. Bull.* **76** 107–12

[15] Zhu T, Fu C, Xie H, Liu Y and Zhao X 2015 High efficiency half-Heusler thermoelectric materials for energy harvesting *Adv. Energy Mater.* **5** 1500588

[16] Plirdpring T, Kurosaki K, Kosuga A, Day T, Firdosy S, Ravi V, Snyder G J, Harnwunggmoung A, Sugahara T and Ohishi Y 2012 Chalcopyrite CuGaTe2: a high-efficiency bulk thermoelectric material *Adv. Mater.* **24** 3622–6

[17] Skoug E J, Cain J D and Morelli D T 2011 High thermoelectric figure of merit in the Cu3SbSe4-Cu3SbS4 solid solution *Appl. Phys. Lett.* **98** 261911

[18] Balke B, Ouardi S, Graf T, Barth J, Blum C G, Fecher G H, Shkabko A, Weidenkaff A and Felser C 2010 Seebeck coefficients of half-metallic ferromagnets *Solid State Commun.* **150** 529–32

[19] Barth J, Fecher G H, Balke B, Ouardi S, Graf T, Felser C, Shkabko A, Weidenkaff A, Klaer P and Elmers H J 2010 Itinerant half-metallic ferromagnets Co 2 Ti Z (Z = Si, Ge, Sn): *Ab initio* calculations and measurement of the electronic structure and transport properties *Physical Review B* **81** 064404

[20] Graf T, Barth J, Balke B, Populoh S, Weidenkaff A and Felser C 2010 Tuning the carrier concentration for thermoelectrical application in the quaternary Heusler compound $Co_2TiAl_{(1-x)}$ Six *Scr. Mater.* **63** 925–8

[21] Graf T, Barth J, Blum C G, Balke B, Felser C, Klaer P and Elmers H-J 2010 Phase-separation-induced changes in the magnetic and transport properties of the quaternary Heusler alloy Co_2Mn_{1-x} Ti x Sn *Physical Review B* **82** 104420

[22] Mohankumar R, Ramasubramanian S, Rajagopalan M, Raja M M, Kamat S and Kumar J 2015 Effect of Fe substitution on the electronic structure, magnetic and thermoelectric properties of Co_2FeSi full Heusler alloy: a first principle study *Comput. Mater. Sci.* **109** 34–40

[23] Reshak A H 2014 Fe_2 MnSi x Ge 1− x: influence thermoelectric properties of varying the germanium content *RSC Adv.* **4** 39565–71

[24] Mirzaei S *et al* 2020 Effect of substrate bias voltage on the composition, microstructure and mechanical properties of W-B-C coatings *Appl. Surf. Sci.* **528** 146966

[25] Schwarz K, Blaha P and Madsen G K H 2002 Electronic structure calculations of solids using the WIEN2k package for material sciences *Comput. Phys. Commun.* **147** 71–6

[26] Sjöstedt E, Nordström L and Singh D J 2000 An alternative way of linearizing the augmented plane-wave method *Solid State Commun.* **114** 15–20

[27] Schwarz K and Blaha P 2003 Solid state calculations using WIEN2k *Comput. Mater. Sci.* **28** 259–73

[28] Perdew J P, Ruzsinszky A, Csonka G I, Vydrov O A, Scuseria G E, Constantin L A, Zhou X and Burke K 2008 Restoring the density-gradient expansion for exchange in solids and surfaces *Phys. Rev. Lett.* **100** 136406

[29] Koller D, Tran F and Blaha P 2012 Improving the modified Becke-Johnson exchange potential *Phys. Rev. B* **85** 155109

[30] Monkhorst H J and Pack J D 1976 Special points for Brillouin-zone integrations *Phys. Rev. B* **13** 5188–92

[31] Jamal M 2014 IRelast and 2DR-optimize packages are provided by M *Jamal As Part of the Commercial Code WIEN2K* http://www.wien2k.at/

[32] Madsen G K H and Singh D J 2006 BoltzTraP. A code for calculating band-structure dependent quantities *Comput. Phys. Commun.* **175** 67–71

[33] Alfè D 2009 PHON: a program to calculate phonons using the small displacement method *Comput. Phys. Commun.* **180** 2622–33

[34] Gulans A, Kontur S, Meisenbichler C, Nabok D, Pavone P, Rigamonti S, Sagmeister S, Werner U and Draxl C 2014 exciting: a full-potential all-electron package implementing density-functional theory and many-body perturbation theory *J. Phys. Condens. Matter* **26** 363202

[35] Langlinais J and Callaway J 1972 Energy bands in ferromagnetic nickel *Phys. Rev. B* **5** 124–34

[36] Kerr J 1877 XLIII. On rotation of the plane of polarization by reflection from the pole of a magnet *The London, Edinburgh, and Dublin Philosophical Magazine and Journal of Science* **3** 321–43

[37] Faraday M 1846 I. Experimental researches in electricity.—Nineteenth series *Philosophical Transactions of the Royal Society of London* **136** 1–20
[38] Feng Z, Zhang J, Yan Y, Zhang G, Wang C, Peng C, Ren F, Wang Y and Cheng Z 2017 Ag–Mg antisite defect induced high thermoelectric performance of α-MgAgSb *Sci. Rep.* **7** 2572
[39] Zheng X F, Liu C X, Yan Y Y and Wang Q 2014 A review of thermoelectrics research—recent developments and potentials for sustainable and renewable energy applications *Renew. Sustain. Energy Rev.* **32** 486–503
[40] Bell L E 2008 Cooling, heating, generating power, and recovering waste heat with thermoelectric systems *Science* **321** 1457
[41] DiSalvo F J 1999 Thermoelectric cooling and power generation *Science* **285** 703
[42] Snyder G J and Toberer E S 2008 Complex thermoelectric materials *Nat. Mater.* **7** 105–14
[43] Shi X, Chen L and Uher C 2016 Recent advances in high-performance bulk thermoelectric materials *Int. Mater. Rev.* **61** 379–415